Provided for non-commercial research and education use.
Not for reproduction, distribution or commercial use.

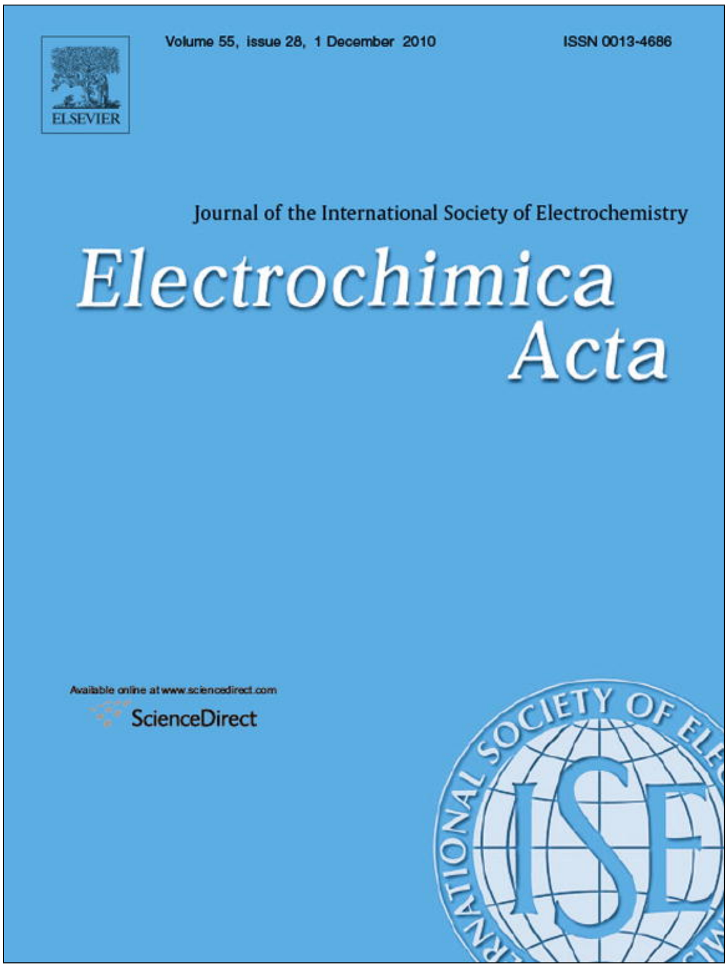

Volume 55, issue 28, 1 December 2010
ISSN 0013-4686

Journal of the International Society of Electrochemistry

Electrochimica Acta

Available online at www.sciencedirect.com
ScienceDirect

This article appeared in a journal published by Elsevier. The attached copy is furnished to the author for internal non-commercial research and education use, including for instruction at the authors institution and sharing with colleagues.

Other uses, including reproduction and distribution, or selling or licensing copies, or posting to personal, institutional or third party websites are prohibited.

In most cases authors are permitted to post their version of the article (e.g. in Word or Tex form) to their personal website or institutional repository. Authors requiring further information regarding Elsevier's archiving and manuscript policies are encouraged to visit:

http://www.elsevier.com/copyright

Electrochimica Acta 55 (2010) 8673–8679

Contents lists available at ScienceDirect

Electrochimica Acta

journal homepage: www.elsevier.com/locate/electacta

Computer simulation of reversible electrochemical catalyst promoter dosing

Mariana I. Rojas, Marcelo M. Mariscal, Ezequiel P.M. Leiva[*,1]

INFIQC, Departamento de Matemática y Física, Fac. de Ciencias Químicas, Universidad Nacional de Córdoba, Ciudad Universitaria, 5000 Córdoba, Argentina

ARTICLE INFO

Article history:
Received 9 February 2010
Received in revised form 14 July 2010
Accepted 17 July 2010
Available online 23 July 2010

Keywords:
Sodium promoter
Platinum oxide surface
Ordered structure
DFT
Grand Canonical Monte Carlo simulations

ABSTRACT

Grand Canonical Monte Carlo simulations were used to study the growth of a Na layer onto a O–$p(2\times2)$–Pt(1 1 1) surface. At the beginning of the deposition, the film presents a disordered structure which becomes progressively ordered as the coverage increases due to the repulsive lateral interactions between the adsorbates. We found some ordered structures like $p(16\times16)$, $p(14\times14)$ and $p(12\times12)$ which appears at coverages l lower than $\Theta\sim0.007$, in all these overlayers the Na adatoms are adsorbed on fcc-hollow sites of the oxide surface.

© 2010 Elsevier Ltd. All rights reserved.

1. Introduction

The catalytic activity of some metallic surfaces deposited on solid electrolytes may be reversibly accelerated or decreased by means of the electrochemical pumping of ions to the catalyst/gas interface (c/g). When the modification of the catalytic activity is higher than that predicted by Faraday's law, the reaction is said to exhibit the NEMCA effect (Non-Faradaic Electrochemical Modification of Catalytic Activity) [1]. This type of modification improves heterogeneous catalytic reactions between adsorbates in contact with the gas phase [1] as well as in aqueous solution [2]. For example, when a Na^+ conductor electrolyte like β''-Al_2O_3 is employed, the negative polarization of the electrode leads to the migration of strongly polarized metal atoms usually represented as $Na^{\delta+}$. Thus, an effective double layer is established, modifying the work function of the metal exposed [1], and affecting the binding strength of reacting adsorbed molecules [3–5].

The catalyst promoters have not only postulated but also visualized using Scanning Tunneling Microscopy (STM). Employing this technique, Vayenas et al [6,7] studied the back spillover of $Na^{\delta+}$promoters on a Pt(1 1 1) single crystal surface. They found that the $Na^{\delta+}$ promoter film presents a $p(12\times12)$ structure, as defined with respect to the Pt(1 1 1) surface. These images provided the first direct confirmations of the spillover phenomena. The Na–$p(12\times12)$ structure was formed on the large O–(2×2)–Pt(1 1 1) terraces after the electrochemically supply of Na^+ ions from the solid electrolyte. The pumping of Na^+ ions is achieved by means of the application of an electric field of about −1 V. This huge field allows extracting the ions from the solid electrolyte which is located next to the surface and pumped them onto the catalyser surface. In the case of $O^{\delta-}$ promoters, a $p(12\times12)$ structure with respect to the Pt(1 1 1) surface has also been observed [8].

In the present work, we studied the growth of a Na layer on a O–$p(2\times2)$–Pt(1 1 1) surface at low coverages (up to $\Theta\sim0.007$) by means of Grand Canonical Monte Carlo simulations. We use this methodology (described more in detail below) because in the Grand Canonical ensemble the chemical potential of the adsorbates (Na atoms) is the external parameter set to control their coverage degree. This is in correspondence with the experimental conditions, where control of the electrochemical potential of the electrons at the catalyst is used to fix the spillover of the Na adatoms. In fact, the chemical potential of the Na atoms μ_{Na} can be written in terms of the electrochemical potentials of Na^+ ions $\tilde{\mu}_{Na^+}$ and the electrochemical potential of the electrons at the working electrode $\tilde{\mu}_e$ as:

$$\mu_{Na}=\tilde{\mu}_{Na^+}+\tilde{\mu}_e \tag{1}$$

Since the Na^+ ions are free to move across the catalyst/solid electrolyte interphase, their chemical potential remains fixed to their bulk value at the latter phase and we have

$$\Delta\mu_{Na}=\Delta\tilde{\mu}_e=\Delta V \tag{2}$$

where the symbol Δ represents the changes and the symbol V denotes the potential applied to the working electrode.

---

[*] Corresponding author. Tel.: +54 351 4344972; fax: +54 351 4344972.
E-mail address: eleiva@fcq.unc.edu.ar (E.P.M. Leiva).

[1] ISE member.

0013-4686/$ – see front matter © 2010 Elsevier Ltd. All rights reserved.
doi:10.1016/j.electacta.2010.07.041

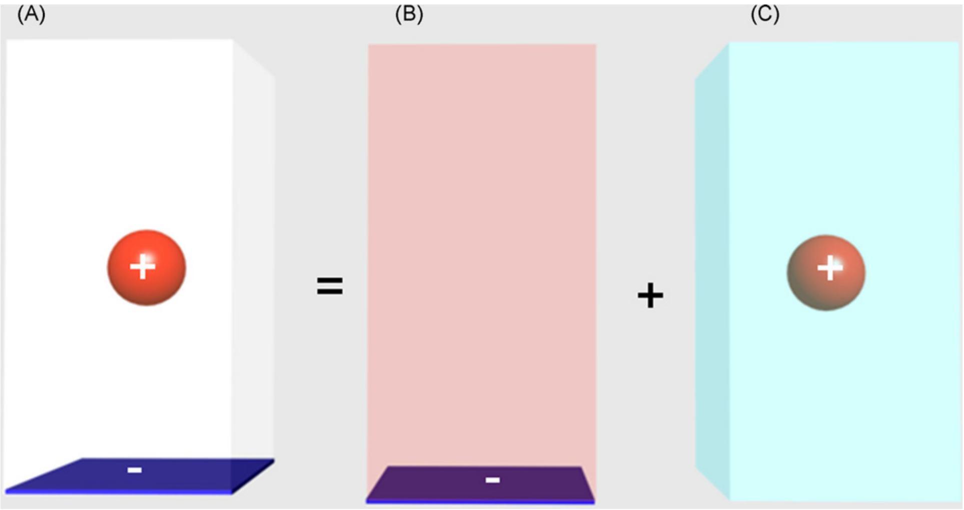

Fig. 1. Scheme of the model employed to calculate the ion/electrode interaction. Blue: negative charge density. Red: positive charge density. (For interpretation of the references to color in this figure legend, the reader is referred to the web version of the article.)

In a previous work [9,10], we studied the adsorption of Na atoms onto a O–$p(2\times 2)$–Pt(1 1 1) surface among other systems by means of density functional theory (DFT) calculations, and determined the charge of all the atoms by the Mulliken population analysis. The $Na^{\delta+}$ atom presented a large charge, close to $\delta = 0.79$ a.u., a value that supports the assumption of a polar-covalent bond. These quantum mechanical calculations provided precise information on atomic scale. Therefore, in order to emulate larger systems, we also performed Grand Canonical Monte Carlo simulations (GCMC) with different approaches to deal with the long-range interactions as: Shifted Potential (SP), Shifted Force (SF) and Damped Shifted Potential (DSP) [11]. With these representations of the electrostatic interactions at different truncation schemes, we studied the structure of the Na^{+} film onto the oxidized platinum surface from the beginning of the adsorption isotherm, up to the completion of the $p(4\times 4)$layer [9,10]. In the present work we present Monte Carlo simulations performed with an improved potential, where the interaction of the adsorbate with the surface is based on first-principles calculations. We find that the presence of corrugation in the potential employed in the simulation leads to the occurrence of commensurate structures of the adsorbate, which resemble the experimental findings.

2. Method and computations

2.1. Interaction potentials

According to our previous studies [9,10], the $Na^{\delta+}$ species present a polar-covalent bond with the surface, with an import charge transfer. Since experience shows that the chemical bonds between atoms are restricted to a few Angstroms, it can be assumed that the main interaction between the $Na^{\delta+}$ ad-species must be mainly of an electrostatic nature. Furthermore, since the charge transfer between the adatoms and the surface is large, it can be expected that the electrostatic contribution is dominant. Thus, we employed the model depicted in Fig. 1. There, we show that the adsorbate/electrode (counter-charge) system (Fig. 1A) is described taking into account the two terms:

$$\underbrace{\frac{\text{negative charge sheet}}{\text{ions}}}_{V_{\text{elec}}} = \underbrace{\frac{\text{negative charge sheet}}{\text{positive charge box}}}_{V^1} + \underbrace{\frac{\text{negative charge box}}{\text{ions}}}_{V^2} \tag{3}$$

Table 1
Electrostatic contribution V_{elec} to the binding energy of Na ad-species on an electrode surface. Its components are described in Eq. (3) and discussed in Fig. 1. The ions were embedded in a tetrahedral box with $L_x = L_y$ and $L_z = 166.3$ Å.

L_x (Å)	V^1 (eV)	V^2 (eV)	V_{elec} (eV)
11.08 (4 × 4)	26.1440	5.9535	32.0975
16.62 (6 × 6)	11.6195	2.3422	13.9617
22.16 (8 × 8)	6.5359	1.1658	7.7017
27.70 (10 × 10)	4.1830	0.6640	4.8470
33.24 (12 × 12)	2.9049	0.4084	3.3133
38.78 (14 × 14)	2.1342	0.0244	2.1586
44.32 (16 × 16)	1.6340	0.0000	1.6340

As we shall see below, this separation is made for computational convenience.

The first term on the right hand side of equation (3) (Fig. 1B) corresponds to the interaction of a negative sheet with a box of uniform positive charge. Employing Gauss' law, the $V^1(r_{ij})$ term can be evaluated and replaced into Eq. (3) to get:

$$V_{\text{elec}} = \frac{q^2 L_z}{6\varepsilon_0 L_x L_y} + V^2 \tag{4}$$

where $q = 0.8$ a.u. is the partial charge on the Na adatoms. The term V^2 corresponds to an ion embedded in a box of homogeneous negative charge (Fig. 1C) and was calculated by Density Functional Theory (DFT) methods employing the SIESTA computer code [12,13]. The results for the evaluation of V_{elec} for a hexagonal ion lattice at different box sizes are listed in Table 1.

On the other hand, DFT calculations show that adsorption of $Na^{\delta+}$ species on O–$p(2\times 2)$–Pt(1 1 1) presents adsorption profiles that are not flat but corrugated in the atomic scale. Thus, to the electrostatic part described in Eq. (3) we must add a corrugation potential that will try to bring the atoms to their equilibrium position. Hence, we can represent the adsorption energy as:

$$E = V_{\text{elec}} + \sum_{i=1}^{n} V_{\text{corr}}(r_i) \tag{5}$$

This equation involves two types of interactions: the first term corresponds to the electrostatic contribution between the adatom and the substrate and between the adatoms themselves, as given by Eq. (3). The second term corresponds to the corrugation potential, denoted with $V_{\mathrm{corr}}(r_i)$.

In order to describe the $V_{\mathrm{corr}}(r_i)$interaction, we employ a 3D potential fitted from DFT calculations as:

$$V_{\mathrm{corr}}(r_i) = (1 - f_1(x_i, y_i)) \cdot f_2(z_i) \cdot \exp(\alpha z_i) \tag{6}$$

where $f_1(x_i,\ y_i)$ is expanded in Fourier series as in the 2D Frenkel–Kontorova's (FK) model:

$$f_1(x_i, y_i) = \sum_{G} V_G \exp(i\vec{G} \cdot \vec{r_{xy}}) \tag{7}$$

where $\vec{G}$ are reciprocal lattice vectors, V_G are the Fourier coefficients of the expansion and $\vec{r_{xy}} = (x_i, y_i)$ is the position of an atom on the surface. This expression is similar to that employed by Pushpa [14] and Hamilton [15].

$$f_1(x_i, y_i) = V_0 + V_1 \sum_{\vec{G} \in G_1} \cos(\vec{G} \cdot \vec{r_{xy}}) + V_2 \sum_{\vec{G} \in G_1} \sin(\vec{G} \cdot \vec{r_{xy}}) + V_3 \sum_{\vec{G} \in G_2} \cos(\vec{G} \cdot \vec{r_{xy}}) \tag{8}$$

where G_1 is a set of three reciprocal lattice vectors of length $4\pi/\sqrt{3}d$ along the x axis and spaced at 120° to the x axis, and G_2 is also a set of three reciprocal lattice vectors of length $4\pi/d$ along the y axis and spaced at 120° to the y axis, $d = 5.54$ Å is the nearest neighbour distance between O atom in the O–$p(2 \times 2)$–Pt(1 1 1) structure.

In order to represent the interaction of Na with the O–$p(2 \times 2)$–Pt(1 1 1) surface given by the $f_1(x_i,y_i)$ function, we determined the V_0, V_1, V_2, V_3 parameters by calculating the total energy of fcc (face centred cubic), hcp (hexagonal closed-packed), bridge and on-top configurations by means of DFT calculations. Exchange and correlation effects were described using a generalized gradient approximation (GGA), within the Perdew–Burke–Ernzerhof (PBE) functional [16] and the same pseudopotentials and parameters described in our previous work [10].

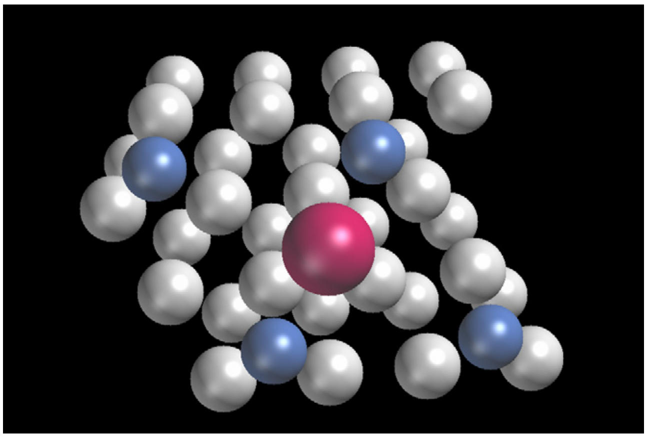

Fig. 2. DFT equilibrium geometry of the Na–$p(4 \times 4)$/O–$p(2 \times 2)$–Pt(1 1 1) system. The Na atom is adsorbed on a fcc-hollow adsorption site. (grey) Pt; (blue) O; (red) Na atom. (For interpretation of the references to color in this figure legend, the reader is referred to the web version of the article.)

Table 2
Relative Na adsorption energies at different surface sites on a O–$p(2 \times 2)$–Pt(1 1 1) surface, referred to the fcc-hollow site (binding energy = −3.03 eV [10]).

Site	Energy (eV)
Hcp	0.040
Bridge	0.053
Top	0.400

The system used is shown in Fig. 2. The binding energy values at the different adsorption sites required to describe $f_1(x_i,y_i)$ are reported in Table 2, referred to the fcc-hollow site which was taken as zero. Fig. 3a–c shows different representations of the $f_1(x_i,y_i)$ function. In Fig. 3a and c it can be observed that the energetic corrugation of the surface is of the order of 0.4 eV. However, Fig. 3c

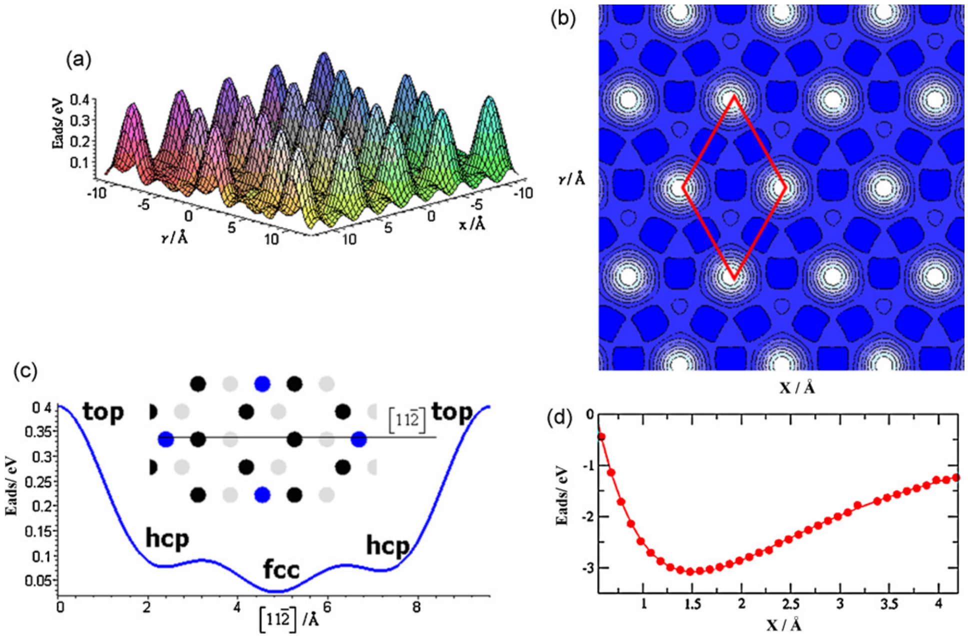

Fig. 3. (a) $f_1(x_i,y_i)$ Fourier series fitting of the interaction potential between Na and a O–$p(2 \times 2)$–Pt(1 1 1) surface. (b) $f_1(x_i,y_i)$ contour plots. The rhombus in red line denotes the $p(2 \times 2)$ structure of the adsorbed O atoms. (c) $f_1(x_i,y_i)$ profile along the $[1\,1\,\bar{2}]$ direction. The characteristic adsorption sites are also indicated. The system geometry and the $[1\,1\,\bar{2}]$ direction are shown in the inset. (Black and grey) Pt atoms in the first and second substrate layers, respectively; (blue) O atom. (d) Na adsorption curve along the direction perpendicular to the surface on a fcc-hollow site. (circle) DFT calculation; (line) least squares fitting.

Table 3
Coefficients a_i of the polynomial $f_2(z_i) = a_4z_i^4 + a_3z_i^3 + a_2z_i^2 + a_1z_i + a_0$ and α exponent of Eq. (6).

Coefficient	Value
a_0	7.7962 eV
a_1	−15.1765 eV Å^{-1}
a_2	0.3343 eV Å^{-2}
a_3	0.3704 eV Å^{-3}
a_4	−0.1960 eV Å^{-4}
α	−1.0074 Å^{-1}

shows that the connection between the fcc and hcp adsorption sites involve very small energy barriers (<0.1 eV) that will be very easily surmounted by the adatoms at room temperature. Fig. 3d shows that binding energy of the Na adatoms to the catalyst surface is larger than 2 eV, denoting a strong attachment to it.

The other part of the interaction potential describes the approaching of the Na atom to the surface and is represented as the product of a fourth order polynomial $f_2(z_i)$ multiplied by an exponential function $\exp(\alpha z_i)$. The $f_2(z_i) \cdot \exp(\alpha z_i)$ contribution is showed in Fig. 3d. This function was fitted from DFT calculations and the parameters are listed in Table 3. Thus, the $V_{\mathrm{corr}}(r_i)$interaction reproduces the surface corrugation which allows the adsorbate to localize on the fcc site as the DFT calculation does.

While the present interaction potential is still approximate since it has not been extracted from a unique DFT calculation, we think that the main contribution the repulsion between the Na$^{\delta+}$ species is present in it, allowing for the presence of the expanded structures, as observed in the experiment. Thus, the present approximation must still be considered a rather heuristic one.

2.2. Simulation method

To mimic the NEMCA experimental system, we consider an open system which is in equilibrium with the environment and exchanges matter and energy with it. In statistical mechanics, the properties of such systems are calculated using the approach of the Grand Canonical ensemble. The strategy of using this ensemble, allows to evaluate properties of systems with fixed μ, V and T from a statistical point of view [24]. Generally speaking, Monte Carlo simulations imply a number of trial/moves that must be related to the conditions imposed to the system. In the particular case of Grand Canonical simulations these moves imply the creation/removal of particles in the system and their motion. In the present case, creation/removal of particles corresponds to the processes of adsorption/desorption of adatoms that take at catalyst surface (system). The coupling to a reservoir with given chemical potential represents the physical connection between the catalyst and the ion source (solid electrolyte).

With the interaction potentials described above we performed computer simulations which were carried out by means of an off-lattice simulation scheme in the Grand Canonical ensemble [17]. In these simulations, the volume (V) of the system and the temperature (T) (equal to 300 K) were fixed, while the chemical potential (μ) of Na species was allowed to take different values (kept constant within a given simulation) between −3.4 eV and 1.75 eV. These conditions were set to simulate the experimental setup, where the potential of the catalyst is fixed by a potentiostat [6], thus determining the chemical potential of the Na species, as discussed above in Eqs. (1) and (2).

The potential energy and the number of Na particles fluctuated according to the different types of events allowed.

2.2.1. Na particle displacement, used as acceptance probability

$$W_{i\to j} = \min\left(1, \exp\left(\frac{-\nu_{ij}}{kT}\right)\right) \tag{9}$$

where ν_{ij} is the change of potential energy related to the configuration change $i \to j$.

In order that high energy barriers, like those for the displacement on the surface, may be overcome by the adatoms, we allowed them to perform “long jumps”, with displacements $\Delta\vec{r}$ according to:

$$\Delta\vec{r} = n_1\vec{s_1} + n_2\vec{s_2} \tag{10}$$

where n_1 and n_2 are integers, and $\vec{s_1}$ and $\vec{s_2}$ are the primitive vectors of the two-dimensional Bravais lattice. These “long jumps” are essential for a proper equilibration of the system during the growth of a layer. “Short jumps”, as usually employed in Monte Carlo simulations where the coordinates of the particles are varied continuously, were also allowed in our studies to describe the vibrational motion of the adsorbate atoms in the neighbourhood of their equilibrium position [18].

2.2.2. Insertion of a Na particle

A particle is randomly inserted into the simulation box and the new configuration is accepted according to:

$$W_{N\to N+1} = \min\left(1, \frac{V}{\Lambda^3(N+1)}\exp\left(\frac{\mu - \Delta\nu_{N+1,N}}{kT}\right)\right) \tag{11}$$

where V is the volume to which the particles have access, $\Lambda = \sqrt{h^2/2\pi mkT}$ is De Broglie’s thermal wavelength, and $\Delta\nu_{N+1,N} = \nu_{N+1} - \nu_N$ denotes the potential energy difference which results from the attempt to create a particle.

2.2.3. Removal of a Na particle

A particle randomly selected is removed from the system and the new configuration is accepted according to:

$$W_{N\to N-1} = \min\left(1, \frac{\Lambda^3 N}{V}\exp\left(\frac{-\mu - \Delta\nu_{N-1,N}}{kT}\right)\right) \tag{12}$$

with $\Delta\nu_{N-1,N} = \nu_{N-1} - \nu_N$.

The relative attempt frequencies of the short hops, long hops, Na adsorption and desorption were 1/4, 1/4, 1/4, and 1/4.

The simulation box was a tetragonal one. Its sides were set equal to $Lx = 33.26$ nm, $L_y = 2L_x\cos(30^\circ)$ and $L_z = 1.5$ nm, and periodic boundary conditions were imposed in the x–y directions.

3. Results and discussion

We carried out a set of Monte Carlo Grand Canonical simulations with the interactions described above. At each chemical potential between −3.4 and 1.75 eV (in 0.05 eV steps), a random distribution of adatoms was generated on the substrate at 300 K and the system was equilibrated for 5000 Monte Carlo steps followed by another 5000 production steps. After this, the system was annealed down to a temperature of 30 K at a rate of 370 MCS K^{-1} to improve the ordering of the adlayer.

Fig. 4 (left) shows the adsorption isotherm (coverage degree Θ vs. μ). As μ becomes more positive (negative polarization of the electrode), the concentration of the Na atoms on the surface increases. Adsorption becomes evident at $\mu = -3.4$ eV and grows steeply, then slowing down.

Fig. 4 (middle) shows the change of adsorption energy per atom as function of the μ. The curve presents a linear behaviour with a slope of 0.27. While the increase of the adsorption energy with the chemical potential is expected on the basis of the repulsive

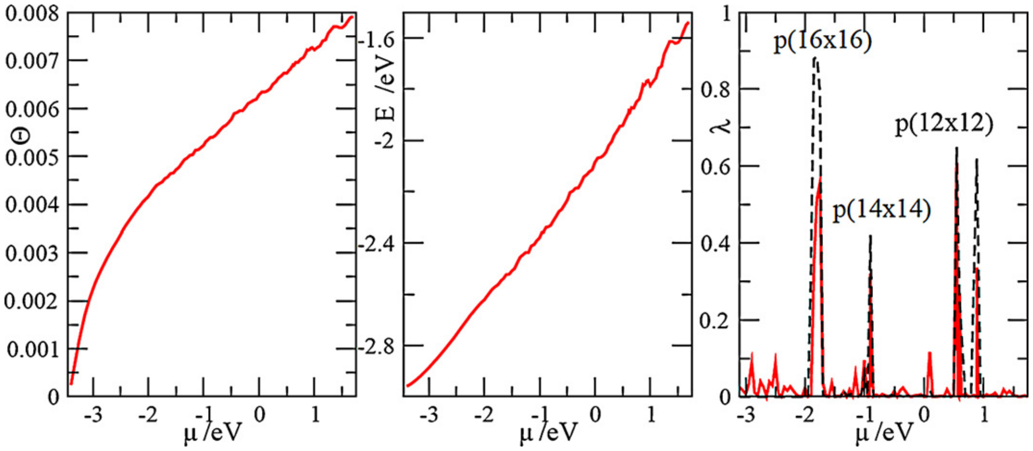

Fig. 4. (left) Coverage degree Θ of Na promoters (referred to the Pt(1 1 1) surface atomic density) (middle) adsorption energy per atom (right) order parameter as function of the chemical potential μ in the interval $[-3.4, 1.75]$ (red continuous line) 300 K (black dashed line) 30 K. (For interpretation of the references to color in this figure legend, the reader is referred to the web version of the article.)

interaction between the adsorbates, we could not derive an expression to relate the energy in terms of μ within the Grand Canonical ensemble. This may be an interest point to tackle in future work.

Fig. 4 (right) shows the translational order parameter as function of μ which was derived according to [20–22]:

$$\lambda(G) = \left\langle \frac{1}{N} \sum_{\vec{r_{ij}}} \exp(i\vec{G} \cdot \vec{r_{ij}}) \right\rangle \tag{13}$$

where N is the number of particles in the system, $\vec{r_{ij}}$ is the vector difference between the instantaneous positions of the particle i and j and the sum run over all the particle pairs.

Here, we rewrite (11) for the general reciprocal lattice vector $\vec{G} = l_1\vec{b_1} + l_2\vec{b_2}$ of the Pt(1 1 1) surface:

$$\lambda(G) = \left\langle \frac{1}{N} \sum_{ij} \cos\left(\frac{2\pi}{a}\left(l_1 \Delta x_{ij} + \left(\frac{l_2}{\sin(\pi/3)} - l_1 \frac{\cos(\pi/3)}{\sin(\pi/3)}\right)\Delta y_{ij}\right)\right)\right\rangle \tag{14}$$

We used $l_1 = 1$ and $l_2 = 1$ to evaluate $\lambda(G)$, but other directions show equivalent results. Δx_{ij} and Δy_{ij} are the components of the $\vec{r_{ij}}$ vector and the lattice parameter a is a function of the coverage obtained assuming a perfect hexagonal lattice for the adsorbate.

λ varies among $0 \le \lambda \le 1$ and is equal to 1 when all the adatoms are forming a perfect commensurate structure with the (1 1 1) layer on the surface. The parameter $\lambda(G)$ was evaluated for this configuration. After this, the system was annealed down to a temperature of 30 K at a rate of 370 MCS K^{-1} and the parameter $\lambda(G)$ was calculated again.

The resulting $\lambda(G)$ vs. μ curve is shown in Fig. 4 (right) at $T = 300$ K and at $T = 30$ K, where the ordering of the different structures becomes more evident. The first maximum, occurring at $\mu = -1.8$ eV was identified as a $p(16 \times 16)$ structure; the next maximum at $\mu = -0.9$ eV corresponds to a $p(14 \times 14)$ overlayer; then at $\mu = -0.6$ eV a $p(12 \times 12)$ structure appears; and finally a $(11.13 \times 11.13)R8^\circ 56'53.79''$ appears. Geometries $p(12 \times 12)$ and $(11.13 \times 11.13)R8^\circ 56'53.79''$ are shown in Fig. 5. Both structures are commensurable with the Na atom on fcc sites.

At the beginning of the adsorption, at low chemical potentials, Na atoms are mainly adsorbed on the fcc sites of the Pt(1 1 1)surface but are disorderly distributed due to thermal diffusion. As shown above in Fig. 3c, the potential energy surface is rather shallow in some directions and the atoms may move relatively free at low coverage. This is the case of the structure observed in Fig. 6a (left) at a chemical potential of -2.60 eV, where the Na atoms are represented as spheres. As these species are positively charged, when the coverage increases the repulsive lateral interactions between Na atoms become stronger and each Na tries to stay away from the other as much as possible. The optimal condition to minimize repulsion is a hexagonal arrangement of the adlayer, and this is the prevailing structure at larger coverages. However, this compact structure is modulated by the potential of the substrate, and this is the reason for the occurrence of the different overlayers observed. Fig. 6a (medium) shows a geometry of the film at a chemical potential of -1.80 eV where the layer present the $p(16 \times 16)$ ordered structure, and Fig. 6a (right) is the $p(12 \times 12)$ structure which appears at 0.60 eV.

A structural analysis of the layer at different chemical potentials was performed in order to study the evolution of the morphology of the film during deposition.

The position of the Na plane was evaluated by means of the average density of particles perpendicular to the surface (S). This quantity was defined in [19] as:

$$g(z) = \frac{\int_S \rho(x, y, z)\,dx\,dy}{S} \tag{15}$$

where $\rho(x, y, z)$ is the one-particle density and z is the direction perpendicular to the surface.

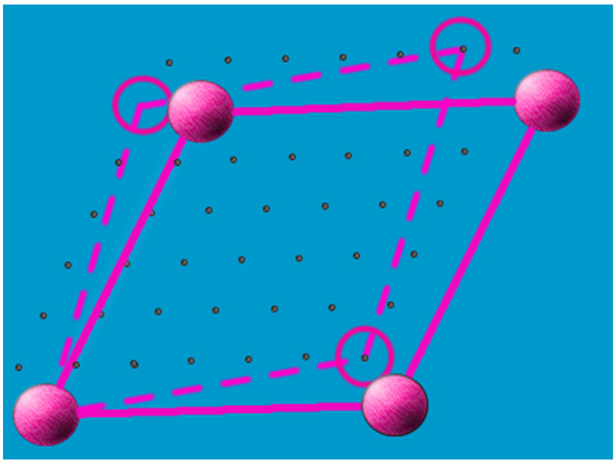

Fig. 5. Shows (full circle, full line) Na–$p(12 \times 12)$ and (empty circle, dashed line) Na – $(11.13 \times 11.13)R8^\circ 56'53.79''$ overlayers.

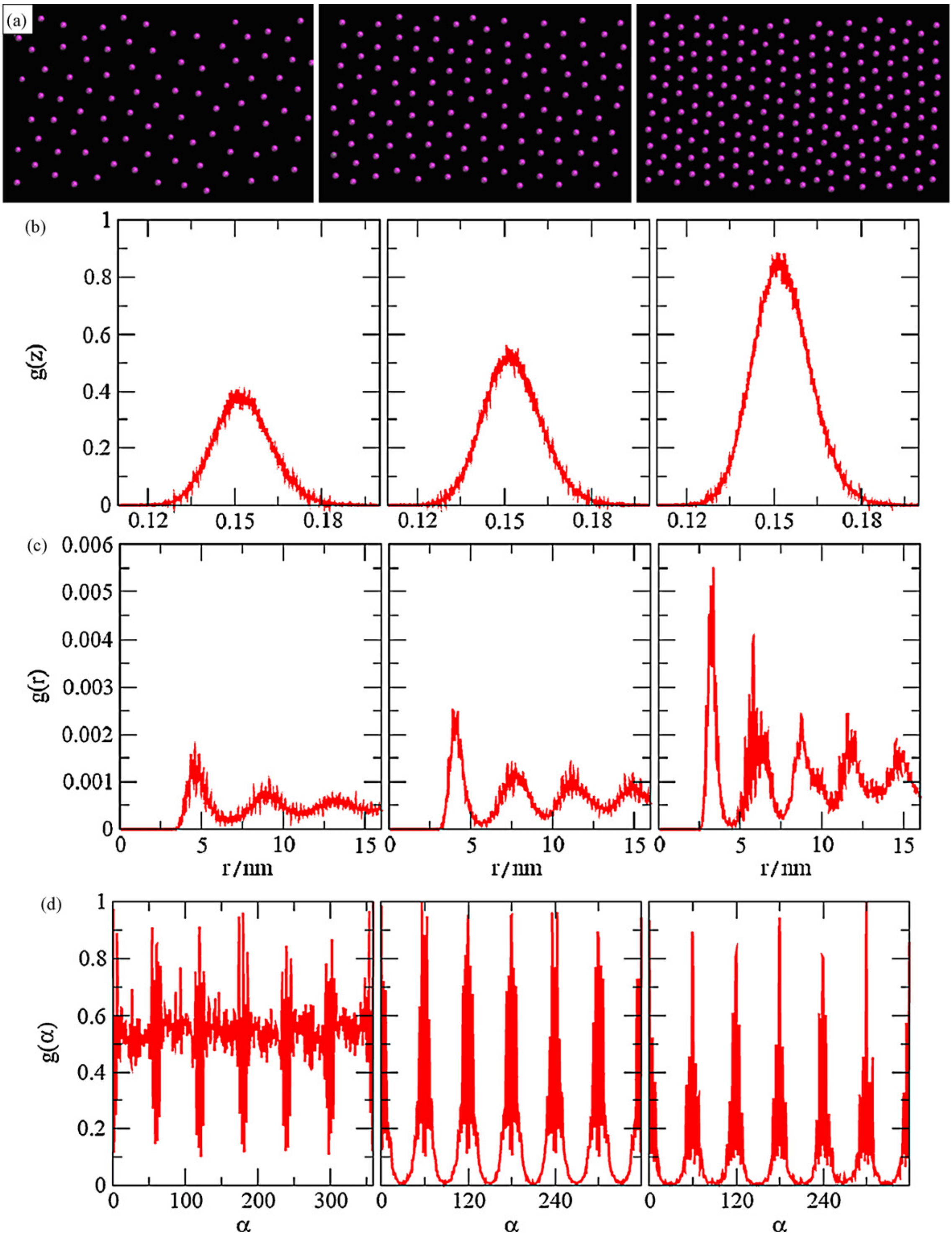

Fig. 6. Results from MC simulation performed at −2.60; −1.80; 0.60 eV chemical potentials. (a) Geometrical configurations where each dot represents an adatom. (b) Average atomic density perpendicular to the surface. (c) Radial distribution function. (d) Angular distribution function.

Fig. 6b shows $g(z)$ distribution for the three chemical potentials considered. Here, the main position of the Na^+ plane appears at 1.58 Å (considering $z = 0$ for the Jellium edge of the metal) and the peak becomes higher and more localized as Θ increases.

To analyze the ordering of the Na particles in the layer we employed the pair distribution function $g(r_{||})$ defined as follows:

$$g(r_{||}) = \frac{S}{N^2}\left\langle \sum_{i}\sum_{j\neq i}\delta\left(r_{||} - \left\|\vec{r_{ij}}\right\|\right)\right\rangle \qquad (16)$$

where $\left\|\vec{r_{ij}}\right\|$ is the projection onto the plane parallel to the surface of the vector $\vec{r_j} - \vec{r_i}$ joining the particles, and S denotes the surface of the system. The averages are taken over cylindrical shells and the distribution function is referred to as an ideal gas with the average surface density N/S [19]. In the present case, the average was calculated from histograms for distances in the range $0 < r_{||} \leq 16$ nm.

Fig. 6c shows that $g(r_{||})$ presents a series of peaks that become higher and more resolved as the chemical potential increases. These peaks correspond to the first, second, third, etc. nearest neighbors of an ordered distribution. With the increase of the coverage, there is a decrease of the nearest neighbour distance in the x–y plane which shows that there is an effect of compression of the film in the x–y direction.

In Fig. 6c (left) the film presents an almost disordered distribution which resembles that of a liquid phase, Fig. 6c (medium) corresponds to the $p(16 \times 16)$ structure and the first maximum appears to 4.43 nm and Fig. 6c (right) corresponds to the $p(12 \times 12)$ with the first maximum located at 3.33 nm. All these ordered structures have even indexes because they grow on the O–$p(2 \times 2)$–Pt(1 1 1) surface.

Furthermore, to complete our structural characterization, we also calculated the angular distribution function of nearest neighbors around a site, $g(\alpha)$. The function $g(\alpha)$ analyzes the possibility of having two neighbors of an atom forming an angle α. The $g(\alpha)$ obtained in the present simulation, shown in Fig. 6d, suggests the occurrence of a hexagonal lattice (angle of 60°) of ions which becomes more resolved as the coverage increases.

The present system shares a number of common features with other systems simulated in the literature, where repulsive interactions between adsorbed particles occur [23]. In this respect, it would be interesting to turn the present off-lattice model into a lattice one, in order to perform a detailed statistical analysis of different phases that arise here. For example, a ground-state analysis (zero-temperature phase diagram) may be useful to identify the different phases that may occur in the system. However, the high mobility of the particles in the present surfaces (also characteristic for the spillover process taking place in the experiment), may make the application of a lattice model not straightforward. On the other hand, the evident next step is the performance of a more detailed study through off-lattice simulations, which is in progress.

4. Conclusions

As observed when the *Na* promoters coverage increases, there is in the film a crossover between a disordered and at least four ordered states, which can be detected from the structural analysis of the simulation results.

During the growth of the film, it is not observed on the surface local patches of sodium particles but it is a homogeneous distribution of them. This is due to the strong repulsive interactions that prevail among the adsorbed particles.

At a chemical potential of 0.60 eV the film presents a $\sim$0.007 coverage with a $p(12 \times 12)$ ordered structure which is in agreement with the experimental measurements [5].

It must be noted that the simple computational model presented here is capable of predicting an important number of qualitative features found in the experiments, opening new perspectives for the simulation of the effective double layer occurring in NEMCA and other related phenomena.

Acknowledgments

This work was supported by PIP 11420090100066 CONICET, Program BID 1728/OC-AR PICT 06-946, PME 2006-1581, SECyT UNC, Argentina. We wish to thank Prof. Constantino Vayenas for providing stimulating disccussion and motivation for the present work.

References

[1] S.G. Neophytides, D. Tsiplakides, P. Stonehart, M.M. Jaksic, C.G. Vayenas, Nature 370 (1994) 45.
[2] C.G. Vayenas, S. Bebelis, S. Ladas, Nature 343 (1990) 625.
[3] C.G. Vayenas, S. Bebelis, I.V. Yentekakis, in: G. Erlt, H. Knötzinger, J. Weitcamp (Eds.), Handbook of Catalysis, VCH, Weinheim, 1997, p. 1310.
[4] C.G. Vayenas, S. Brosda, Solid State Ionics 154–155 (2002) 243.
[5] C.G. Vayenas, S. Brosda, C. Pliangos, J. Catal. 216 (2003) 487.
[6] M. Makri, C.G. Vayenas, S. Bebelis, K.H. Besocke, C. Cavalca, Surf. Sci. 369 (2001) 351.
[7] D. Tsiplakides, C.G. Vayenas, J. Electrochem. Soc. 148 (5) (2001) E189.
[8] C.G. Vayenas, D. Archonta, D. Tsiplakides, J. Electroanal. Chem. 554–555 (2003) 301.
[9] E.P.M. Leiva, C. Vázquez, M.I. Rojas, M.M. Mariscal, OREPOC Conference Proceedings Book 10, 2007.
[10] E.P.M. Leiva, C. Vázquez, M.I. Rojas, M.M. Mariscal, J. Appl. Electrochem. 38 (2008) 1065.
[11] C.J. Fennell, J.D. Gezelter, J. Phys. Chem. 124 (2006) 34104.
[12] P. Ordejón, E. Artacho, J.M. Soler, Phys. Rev. B 53 (1996) R10441.
[13] J.M. Soler, E. Artacho, J.D. Gale, A. García, J. Junquera, P. Ordejón, D. Sánchez-Portal, J. Phys.: Condens. Matter 14 (2002) 2745.
[14] R. Pushpa, S. Narasimhan, Bull. Mater. Sci. 26 (2003) 91.
[15] J.C. Hamilton, R. Stumpf, K. Brumann, M. Giovannini, K. Kern, H. Brune, Phys. Rev. Lett. 82 (1999) 4488.
[16] J.P. Perdew, K. Burke, M. Ernzerhof, Phys. Rev. Lett. 77 (1996) 3865.
[17] D. Frenkel, B. Smit, Understanding Molecular Simulations, Academic Press, London, 1996, p. 101.
[18] M.I. Rojas, M.G. Del Pópolo, E.P.M. Leiva, Langmuir 16 (2000) 9539.
[19] M.P. Allen, D.J. Tildesley, Computer Simulation of Liquids, Oxford University Press, New York, USA, 1992, p. 55.
[20] N.W. Ashcroft, N.D. Mermin, Solid State Physics, Holt Rinehart and Winston, USA, 1976, p. 762.
[21] C. Udink, J. Van der Elsken, Phys. Rev. B 35 (1987) 279.
[22] D.R. Nelson, B.I. Halperin, Phys. Rev. B 19 (1979) 2457.
[23] S.J. Mitchell, G. Brown, P.A. Rikvold, Surf. Sci. 471 (2001) 125.
[24] T.L. Hill, Statistical Mechanics. Principles and Selected Applications, McGraw-Hill, New York, USA, 1987, p. 13.